Single-Layer Limit of Metallic Indium Overlayers on Si(111)

Jae Whan Park and Myung Ho Kang*
Department of Physics, Pohang University of Science and Technology, Pohang 790-784, Korea
(Received 6 April 2016; published 8 September 2016)

Density-functional calculations are used to identify one-atom-thick metallic In phases grown on the Si(111) surface, which have long been sought in quest of the ultimate two-dimensional (2D) limit of metallic properties. We predict two metastable single-layer In phases, one $\sqrt{7} \times \sqrt{3}$ phase with a coverage of 1.4 monolayer (ML; here 1 ML refers to one In atom per top Si atom) and the other $\sqrt{7} \times \sqrt{7}$ phase with 1.43 ML, which indeed agree with experimental evidences. Both phases reveal quasi-1D arrangements of protruded In atoms, leading to 2D-metallic but anisotropic band structures and Fermi surfaces. This directional feature contrasts with the free-electron-like In-overlayer properties that are known to persist up to the double-layer thickness, implying that the ultimate 2D limit of In overlayers may have been achieved in previous studies of double-layer In phases.

DOI: 10.1103/PhysRevLett.117.116102

How thin can metal films be yet retaining the two-dimensional (2D) nature of their metallic properties [1,2]? One atomic layer might be such an ultimate 2D limit. This fundamental question is in fact the very motivation underlying extensive experimental studies of the In [3–16] and Pb [8,13,17–22] overlayers grown on the Si(111)-$(\sqrt{7} \times \sqrt{3})$ surface, which have long been considered to represent one-atom-thick metal overlayers [3,4,17,18]. Especially, for the In/Si(111) $-$ $(\sqrt{7} \times \sqrt{3})$ system, fascinating 2D electronic features were reported, including the free-electron-like parabolic bands and circular Fermi surfaces [6], the persistence of superconductivity with a high T_c close to the bulk value [8,9], and the intriguing metallic transport behavior [10], all of which have been referred to as revealing the ultimate 2D limit.

Unlike the expectations, however, the In/Si(111) $-$ $(\sqrt{7} \times \sqrt{3})$ surface was recently verified by density-functional theory (DFT) calculations [23,24] to actually represent two-atom-thick In overlayers, either rectangular (hereafter, $\sqrt{7}$ rect) or hexagonal ($\sqrt{7}$ hex), with 2.4 ML In coverage. So far, there are two single-layer In phases with the coverage verified as 1.0 ML. One is the 4×1 phase, which is metallic but definitely one dimensional with weakly coupled In chains [25–27], and the other 2×2 phase is known as an insulating 2D honeycomb lattice [7,28,29]. The single-layer limit of 2D metallic In overlayers is not yet identified, and thus it remains an open question whether the 2D free-electron nature of In overlayers persists even in the single-layer limit, or it requires a certain buffer layer to screen the Si substrate effects, as graphene needs at least one buffer layer to recover rather ideal Dirac-cone structures when grown on strongly interacting substrates such as SiC(001) [30,31].

Noteworthy in this regard is that there is *another* In/Si(111) $-$ $(\sqrt{7} \times \sqrt{3})$ surface, differing from the verified $\sqrt{7}$-rect and $\sqrt{7}$-hex double-layer phases. This intermediate phase appears in between the 2×2 and $\sqrt{7}$-rect phases when prepared by room-temperature (RT) In deposition onto the In/Si(111) $-$ $(\sqrt{3} \times \sqrt{3})$ surface and is known to transform into the honeycomblike $\sqrt{7} \times \sqrt{7}$ phase during cooling down in the range from 265 to 225 K [7]. This RT $\sqrt{7} \times \sqrt{3}$ phase was regarded as the $\sqrt{7}$-hex phase on the basis of similar STM images [7], but a recent DFT study clarified that it should be distinguished from the double-layer $\sqrt{7}$-hex phase [24]. Moreover, in a latest STM study [16], the RT $\sqrt{7} \times \sqrt{3}$ phase was clearly identified as the so-called *striped* phase, appearing as a minor phase coexisting with the 1.0-ML 4×1 phase at high-temperature (~400 °C) preparations [4]. In microscopy studies, the striped $\sqrt{7} \times \sqrt{3}$ phase (hereafter, $\sqrt{7}$ stripe) appears 0.5 Å higher than the single-layer 4×1 phase [12] but substantially lower by 1.9 Å than the double-layer $\sqrt{7}$-hex phase [16]. This suggests that the $\sqrt{7}$-stripe phase is possibly one atom thick, but its actual In coverage and structure are not known.

In this Letter, we use DFT calculations to identify single-layer metallic In phases on Si(111). Our formation-energy calculations predict two metastable In phases, one 1.4-ML $\sqrt{7} \times \sqrt{3}$ phase and the other 1.43-ML $\sqrt{7} \times \sqrt{7}$ phase, which agree well with the aforementioned $\sqrt{7}$-stripe and $\sqrt{7} \times \sqrt{7}$ surfaces, respectively. Both phases reveal interesting quasi-1D structural features with protruded In atoms, leading to anisotropic 2D-metallic band structures. Their electronic nature will be compared with those of the established double-layer In phases.

We perform DFT calculations by using the Vienna *ab initio* simulation package [32] within the Perdew-Burke-Ernzerhof generalized gradient approximation [33] and the projector augmented wave method [34]. The

Si(111) surface is modeled by a periodic slab geometry with a slab thickness of 6 atomic layers and a vacuum spacing of about 12 Å. The calculated value 2.370 Å is used as the bulk Si-Si bond length. Indium atoms are adsorbed on the top of the slab, and the bottom is passivated by H atoms. We use a plane-wave basis set of 246 eV and a $4 \times 6 \times 1$ k-point mesh for the $\sqrt{7} \times \sqrt{3}$ unit cell. All atoms but the bottom two Si layers are relaxed until the residual force components are within 0.01 eV/Å. Similar calculation schemes were successfully used in our In/Si(111) studies [23,24].

We first examine the energy stability of In overlayers on Si(111) $-$ $(\sqrt{7} \times \sqrt{3})$ in the coverage range of 1.0–2.4 ML, by regarding the 1.0 ML of the 2×2 phase and the 2.4 ML of the $\sqrt{7}$-rect phase as the lower and upper bounds, respectively. For a given In coverage, we try various In configurations and identify the lowest-energy structure by comparing their formation energies, defined by $E = E_{\mathrm{In/Si}} - E_{\mathrm{Si}} - N \times E_{\mathrm{In}}$, where $E_{\mathrm{In/Si}}$, E_{Si}, and E_{In} are the total energies of the In/Si(111) $-$ $(\sqrt{7} \times \sqrt{3})$ surface, the Si(111) $-$ $(\sqrt{7} \times \sqrt{3})$ surface, and the bulk In atom, respectively, and N is the number of In atoms per $\sqrt{7} \times \sqrt{3}$ unit cell.

Figure 1 shows two energy curves obtained by using different In-covered substrates. One starting configuration was the 1.2-ML rectangular In phase shown in Fig. 1(a), which could be a precursor layer to the saturated double-layer (i.e., 2.4-ML $\sqrt{7}$-rect) phase. We searched the lowest-energy structures with increasing In atoms one by one (for the detail, see the Supplemental Material [35]). The resulting energy curve (denoted by open circles) is getting lower with In coverage until arriving at the 2.4-ML $\sqrt{7}$-rect phase, which is known as a thermodynamically stable phase [23]. The other starting configuration was the 1.0-ML hexagonal In phase shown in Fig. 1(b), which is also considerable as a precursor layer perfectly matching the Si(111) $-$ (1×1) surface. The resulting energy curve (filled circles) shows an interesting coverage dependence. Whereas the final 2.0-ML double-layer phase appears very unstable, the lower-coverage phases are relatively stable with lower formation energies than the above-mentioned 1.2-ML series. Moreover, there is a unique local-energy minimum at 1.4 ML, implying a metastable In phase. This 1.4-ML phase has a relatively low formation energy (0.05 eV lower than the 1.0-ML 2×2 phase and 0.16 eV higher than the 1.0-ML 4×1 phase per $\sqrt{7} \times \sqrt{3}$ unit cell) and thus becomes a candidate for the $\sqrt{7}$-stripe phase that usually appears together with the 4×1 or 2×2 phase in experiments [4,7].

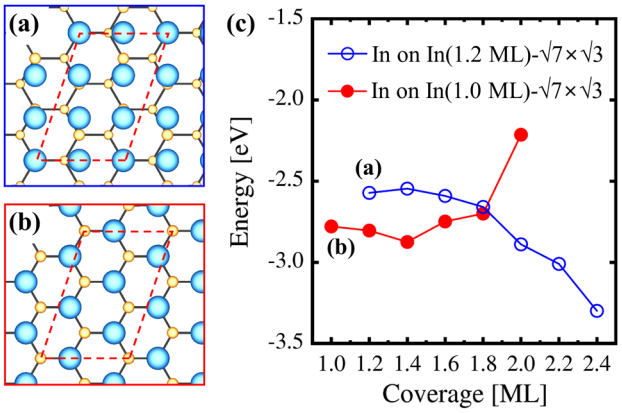

FIG. 1. Formation energy as a function of In coverage obtained from different initial substrates: (a) 1.2-ML rectangular and (b) 1.0-ML hexagonal In/Si(111)-$(\sqrt{7} \times \sqrt{3})$, where large (small) balls represent In (Si) atoms. Additional In atoms are tried on the hollow sites of (a) and (b), and the energy of the most stable configuration in each coverage is shown in (c).

Figure 2 shows the atomic structure of the 1.4-ML phase. Of the seven In atoms per $\sqrt{7} \times \sqrt{3}$ unit cell, five (denoted by light blue) strongly interact with the top Si atoms with an average interlayer spacing of 2.66 Å, whereas the remaining two (dark blue) are a little more protruded by 0.91 Å. The In coverage 1.4 ML is higher than 1.19 ML of the In(001) single layer but far lower than 2.4 ML of the double-layer $\sqrt{7} \times \sqrt{3}$ structures, and the layer puckering of 0.91 Å is much smaller than the interlayer spacing of 2.40 Å of the double-layer structures [23,24]. Thus, the 1.4-ML In phase may well be regarded as a dense single layer.

The 1.4-ML phase indeed accounts well for the microscopic features of the $\sqrt{7}$-stripe surface [4,7,16]. As seen in Fig. 2(b), its STM simulation compares well with the reported STM image of the $\sqrt{7}$-stripe surface [7]: The protruded In atoms form a bright zigzag pattern along the $\sqrt{3}$ direction in good agreement with the experimental

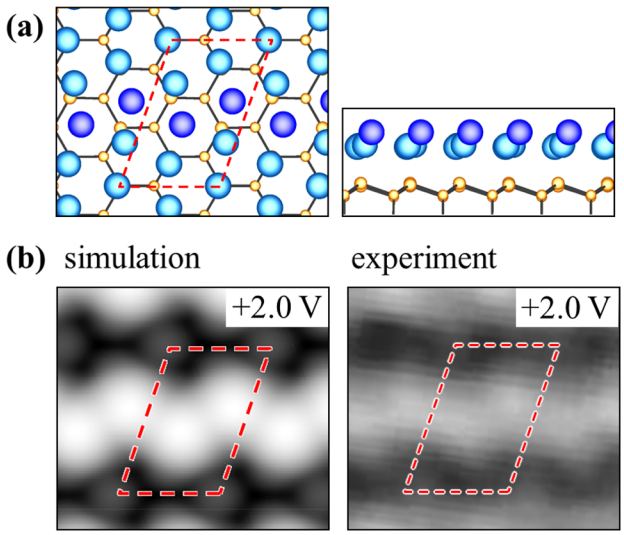

FIG. 2. 1.4-ML In/Si(111)-$(\sqrt{7} \times \sqrt{3})$. (a) Atomic structure and (b) Simulated STM image, representing the surface of constant density with $\rho = 1 \times 10^{-3}$ $e/\mathrm{Å}^3$. The experimental image was taken from Ref. [7].

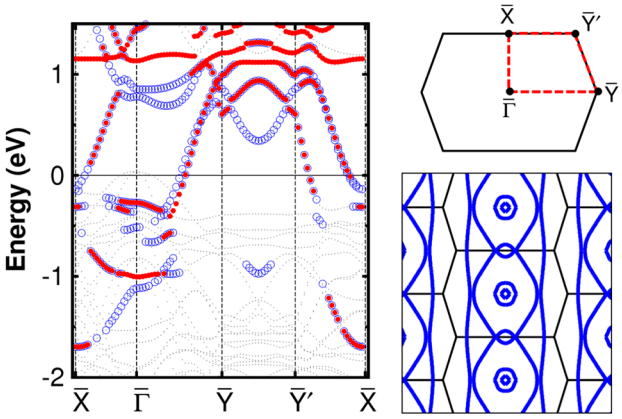

FIG. 3. Band structure of the $\sqrt{7}$-stripe phase. Filled (open) circles represent In-derived states containing more than 20% of charge in the protruded In atoms (more than 40% in the other In atoms). The $\sqrt{7} \times \sqrt{3}$ Brillouin zone and the calculated Fermi contours are shown in the right panel.

stripe image. The 1.4-ML phase is also compatible with the reported topographic heights of the $\sqrt{7}$-stripe surface. The height difference of 0.5 Å between the $\sqrt{7}$-stripe and 4×1 surfaces, measured by atomic force microscopy [12], is close to our calculation of 0.36 Å from the atomic heights of the 1.4-ML and 4×1 phases. The STM height difference of 1.9 Å between the $\sqrt{7}$-stripe and $\sqrt{7}$-hex surfaces [16] also compares well with our calculations of 1.54 Å in atomic structure and 1.89 Å in STM topograph. Hereafter, we refer to the 1.4-ML phase as the $\sqrt{7}$-stripe phase.

Figure 3 shows the electronic structure of the $\sqrt{7}$-stripe phase. This single-layer In phase is 2D metallic with multiple bands crossing the Fermi level, but its 2D band structure is certainly anisotropic, well reflecting its quasi-1D structural character: It features two noticeable metallic bands with large dispersion along both $\bar{\Gamma}$-to-$\bar{Y}$ and $\bar{Y}'$-to-$\bar{X}$ lines (parallel to the zigzag In-chain direction), whereas the metallic nature is much weaker along the $\bar{\Gamma}$-to-$\bar{X}$ and $\bar{Y}$-to-$\bar{Y}'$ lines. The band gap along the $\bar{Y}$-to-$\bar{Y}'$ line is well reflected in the anisotropic Fermi contours. This quasi-1D electronic nature is in contrast with the 2D free-electron-like features of the double-layer ($\sqrt{7}$-rect and $\sqrt{7}$-hex) phases [23,24].

It is interesting to further identify the $\sqrt{7} \times \sqrt{7}$ phase that is transformed from the $\sqrt{7}$-stripe phase at low temperatures (LTs) of 225–265 K [7]. We extended our formation-energy calculations for the $\sqrt{7} \times \sqrt{7}$ unit cell in the coverage range of 1.0–2.0 ML (for the detail, see the Supplemental Material [35]) and found a unique local-energy minimum at 1.43 ML (corresponding to 10 In atoms per $\sqrt{7} \times \sqrt{7}$ unit cell). As seen in Fig. 4, this 1.43-ML $\sqrt{7} \times \sqrt{7}$ phase also retains a quasi-1D structural nature with protruded In atoms, similar to the $\sqrt{7}$-stripe phase but with a different chain direction. Fascinating is its simulated

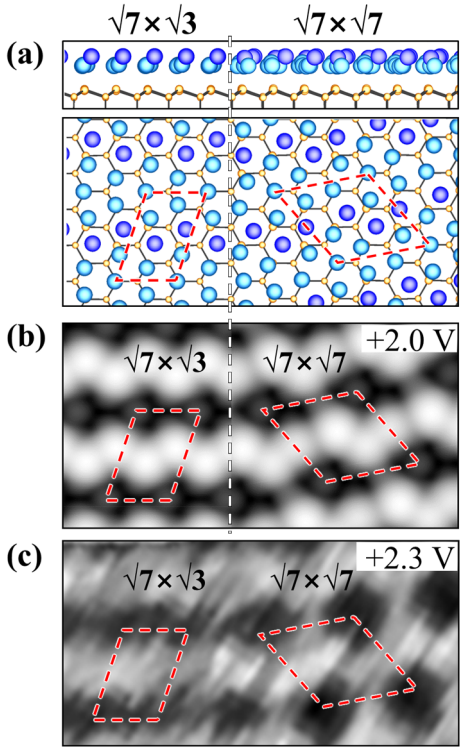

FIG. 4. Phase boundary between the 1.4-ML $\sqrt{7}$-stripe and 1.43-ML $\sqrt{7} \times \sqrt{7}$ phases: (a) Atomic structure, (b) simulated STM image, and (c) experimental STM image taken from Ref. [7].

STM image that reproduces well not only the experimental honeycomblike image of the LT $\sqrt{7} \times \sqrt{7}$ phase but also the sharp phase boundary with the coexisting $\sqrt{7}$-stripe phase [7]. We readily identify the 1.43-ML phase as the LT $\sqrt{7} \times \sqrt{7}$ phase. This assignment is also sound energetically: The 1.43-ML phase has a lower formation energy (by 0.10 eV per $\sqrt{7} \times \sqrt{3}$ unit cell) than the 1.4-ML $\sqrt{7}$-stripe phase, accounting well for the preference of the $\sqrt{7} \times \sqrt{7}$ phase at low temperatures. At elevated temperatures, however, the 1.4 ML $\sqrt{7}$-stripe phase would be favorable with a slightly lower In coverage because In has a much larger thermal expansion coefficient (32.1×10^{-6}/K in the bulk) than Si (2.6×10^{-6}/K in the bulk) [36,37].

In their recent DFT study, Mihalyuk *et al.*. proposed structural models for the $\sqrt{7} \times \sqrt{7}$ phase [38]. We find, however, that the proposed models reflect only one In coverage of 1.14 ML, driven by the wrong assumption that the $\sqrt{7} \times \sqrt{3}$-stripe phase has an In coverage of 1.2 ML, and thus are less stable than our 1.43-ML phase (see the Supplemental Material [35]).

Figure 5 shows the electronic structure of the $\sqrt{7} \times \sqrt{7}$ phase. The 2D-metallic band structure is also anisotropic with dispersive metallic bands along the $\bar{\Gamma}$-to-$\bar{K}$ line and a nondispersive metallic band along the $\bar{\Gamma}$-to-$\bar{M}$ direction, and so are the Fermi contours.

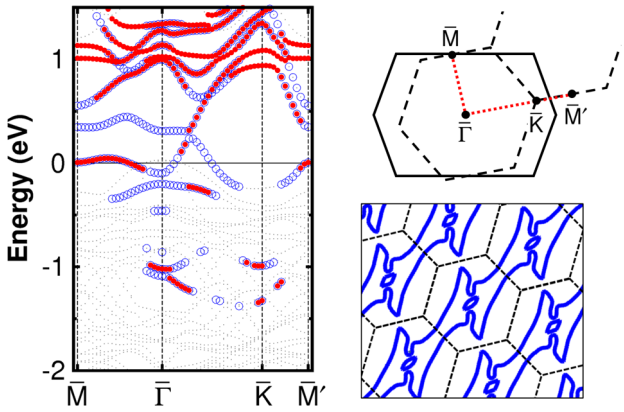

FIG. 5. Band structure of the $\sqrt{7}\times\sqrt{7}$ phase. The $\sqrt{7}\times\sqrt{7}$ Brillouin zone (dashed lines) and the calculated Fermi contours are shown in the right panel.

Figure 6 shows the In-derived local density of states (LDOS) of the $\sqrt{7}$-stripe and $\sqrt{7}\times\sqrt{7}$ phases. Both phases reveal almost the same LDOS spectra, well reflecting their similar In coverages and quasi-1D structural nature. Their LDOS spectra, however, differ clearly from those of the double-layer phases. The main peaks located at about −0.55 eV are much higher in energy than the peaks of the double-layer phases (at about −0.90 eV), indicating that the higher (i.e., less stable) In levels in the single-layer phases are shifted to lower (i.e., more stable) levels in the double-layer phases: Unlike the less stable single-layer phases, the double-layer phases are known to almost recover the stable bulk properties in both atomic and electronic structure [23]. It is also noticeable that the single-layer phases have much weaker LDOS values at the Fermi level than the double-layer phases, implying that the free-electron-like nature of In overlayers is greatly suppressed in the single-layer regime by the dominant Si-In interactions.

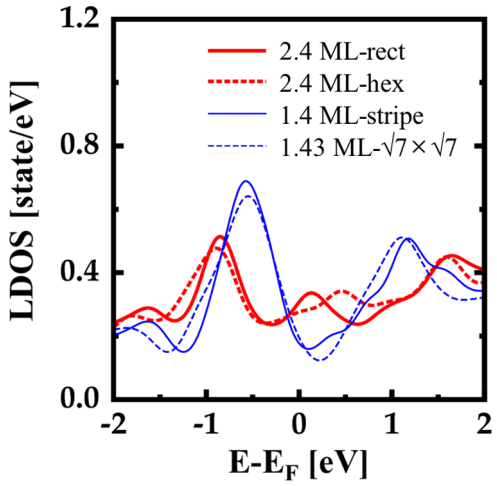

FIG. 6. Layer-resolved density of states per In atom for the single- and double-layer indium phases.

In conclusion, the striped In/Si(111) − $\sqrt{7}\times\sqrt{3}$ phase and its low-temperature $\sqrt{7}\times\sqrt{7}$ phase represent one-atom-thick metallic In overlayers, but their quasi-1D structural features result in anisotropic 2D band structures and Fermi surfaces, which contrast with those of the double layer In phases that still retain the free-electron-like metallic properties [23,24]. This strongly suggests that the ultimate 2D limit of free-electron-like In overlayers on Si(111) could be In double layers. At least one buffer layer may be needed to screen the rather strong substrate interactions, exactly as the Dirac cone of graphene is realized not in monolayers but in bilayers or by proper intercalations, when grown on strongly interacting SiC(001) [30,31] and Ni(111) [39,40] surfaces.

This work was supported by the National Research Foundation of Korea (Grant No. 2011-0008907).

*kang@postech.ac.kr

[1] K. Fuchs, The conductivity of thin metallic films according to the electron theory of metals, Proc. Cambridge Philos. Soc. **34**, 100 (1938).
[2] C. R. Tellier and A. J. Tosser, *Size Effects in Thin Films* (Elsevier, New York, 1982).
[3] J. Kraft, S. L. Surnev, and F. P. Netzer, The structure of the indium-Si(111)($\sqrt{7}\times\sqrt{3}$) monolayer surface, Surf. Sci. **340**, 36 (1995).
[4] J. Kraft, M. G. Ramsey, and F. P. Netzer, Surface reconstructions of In on Si(111), Phys. Rev. B **55**, 5384 (1997).
[5] I. G. Hill and A. B. McLean, Strongly anisotropic band dispersion of an image state located above metallic nanowires, Phys. Rev. Lett. **82**, 2155 (1999).
[6] E. Rotenberg, H. Koh, J. Rossnagel, H. W. Yeom, J. Schäfer, B. Krenzer, M. P. Rocha, and S. D. Kevan, Indium $\sqrt{7}\times\sqrt{3}$ on Si(111): A nearly free electron metal in two dimensions, Phys. Rev. Lett. **91**, 246404 (2003).
[7] A. A. Saranin, A. V. Zotov, M. Kishida, Y. Murata, S. Honda, M. Katayama, K. Oura, D. V. Gruznev, A. Visikovskiy, and H. Tochihara, Reversible phase transitions in the pseudomorphic $\sqrt{7}\times\sqrt{3}$-hex In layer on Si(111), Phys. Rev. B **74**, 035436 (2006).
[8] T. Zhang, P. Cheng, W.-J. Li, U.-J. Sun, G. Wang, X.-G. Zhu, K. He, L. Wang, X. Ma, X. Chen, Y. Wang, Y. Liu, H.-Q. Lin, J.-F. Jia, and Q.-K. Xue, Superconductivity in one-atomic-layer metal films grown on Si(111), Nat. Phys. **6**, 104 (2010).
[9] T. Uchihashi, P. Mishra, M. Aono, and T. Nakayama, Macroscopic superconducting current through a silicon surface reconstruction with indium adatoms: Si(111)-($\sqrt{7}\times\sqrt{3}$)-In, Phys. Rev. Lett. **107**, 207001 (2011).
[10] S. Yamazaki, Y. Hosomura, I. Matsuda, R. Hobara, T. Eguchi, Y. Hasekawa, and S. Hasegawa, Metallic transport in a monatomic layer of In on a silicon surface, Phys. Rev. Lett. **106**, 116802 (2011).
[11] S. H. Uhm and H. W. Yeom, Electron-phonon interaction of one-dimensional and two-dimensional surface states in indium adlayers on the Si(111) surface, Phys. Rev. B **86**, 245408 (2012).

[12] K. Iwata, S. Yamazaki, Y. Tani, and Y. Sugimoto, Mechanical properties of various phases on In/Si(111) surfaces revealed by atomic force microscopy, Appl. Phys. Express **6**, 055201 (2013).
[13] M. Yamada, T. Hirahara, and S. Hasegawa, Magnetoresistance measurements of a superconducting surface state of In-induced and Pb-induced structures on Si(111), Phys. Rev. Lett. **110**, 237001 (2013).
[14] T. Uchihashi, P. Mishra, and T. Nakayama, Resistive phase transition of the superconducting Si(111)-$(\sqrt{7}\times\sqrt{3})$-In surface, Nanoscale Res. Lett. **8**, 167 (2013).
[15] S. Yoshizawa, H. Kim, T. Kawakami, Y. Nagai, T. Nakayama, X. Hu, Y. Hasegawa, and T. Uchihashi, Imaging Josephson vortices on the surface superconductor Si(111)-$(\sqrt{7}\times\sqrt{3})$-In using a scanning tunneling microscope, Phys. Rev. Lett. **113**, 247004 (2014).
[16] D. Shin, J. Woo, Y. Jeon, H. Shim, and G. Lee, Investigation of $\sqrt{7}\times\sqrt{3}$ structures grown on In/Si(111) surface at room temperature, J. Korean Phys. Soc. **67**, 1192 (2015).
[17] K. Horikoshi, X. Tong, T. Nagao, and S. Hasegawa, Structural phase transitions of Pb-adsorbed Si(111) surfaces at low temperatures, Phys. Rev. B **60**, 13287 (1999).
[18] C. Kumpf, O. Bunk, J. H. Zeysing, M. M. Nielsen, M. Nielsen, R. L. Johnson, and R. Feidenhans'l, Structural study of the commensurate-incommensurate low-temperature phase transition of Pb on Si(111), Surf. Sci. **448**, L213 (2000).
[19] S. Qin, J. Kim, Q. Niu, and C.-K. Shih, Superconductivity at the two-dimensional limit, Science **324**, 1314 (2009).
[20] S. Kim, S. C. Jung, M. H. Kang, and H. W. Yeom, Nearly massless electrons in the silicon interface with a metal film, Phys. Rev. Lett. **104**, 246803 (2010).
[21] C. Brun, T. Cren, V. Cherkez, F. Debontridder, S. Pons, D. Fokin, M. C. Tringides, S. Bozhko, L. B. Ioffe, B. L. Altshuler, and D. Roditchev, Remarkable effects of disorder on superconductivity of single atomic layers of lead on silicon, Nat. Phys. **10**, 444 (2014).
[22] A. Stępniak, A. L. Vanegas, M. Caminale, H. Oka, D. Sander, and J. Kirshner, Atomic layer superconductivity, Surf. Interface Anal. **46**, 1262 (2014).
[23] J. W. Park and M. H. Kang, Double-layer In structural model for the In/Si(111) $-\sqrt{7}\times\sqrt{3}$ surface, Phys. Rev. Lett. **109**, 166102 (2012).
[24] J. W. Park and M. H. Kang, Hexagonal indium double layer on Si(111)-$\sqrt{7}\times\sqrt{3}$ surface, Phys. Rev. B **92**, 045306 (2015).
[25] H. W. Yeom, S. Takeda, E. Rotenberg, I. Matsuda, J. Schaefer, C. M. Lee, S. D. Kevan, T. Ohta, T. Nagao, and S. Hasegawa, Instability and charge density wave of metallic quantum chains on a silicon surface, Phys. Rev. Lett. **82**, 4898 (1999).
[26] O. Bunk, G. Falkenberg, J. H. Zeysing, L. Lottermoser, R. L. Johnson, M. Nielsen, F. Berg-Rasmussen, J. Baker, and R. Feidenhas'l, Structure determination of the indium-induced Si(111)-(4×1) reconstruction by surface x-ray, Phys. Rev. B **59**, 12228 (1999).
[27] J.-H. Cho, D.-H. Oh, K. S. Kim, and L. Kleinman, Weakly correlated one-dimensional indium chains on Si(111), Phys. Rev. B **64**, 235302 (2001).
[28] J. P. Chou, C. M. Wei, Y. L. Wang, D. V. Gruznev, L. V. Bondarenko, A. V. Matetskiy, A. Y. Tupchaya, A. V. Zotov, and A. A. Saranin, Atomic structure and electronic properties of the In/Si(111)2×2 surface, Phys. Rev. B **89**, 155310 (2014).
[29] S. G. Kwon and M. H. Kang, Honeycomb network of indium trimers and monomers on Si(111)-(2×2), Phys. Rev. B **89**, 165304 (2014).
[30] T. Ohta, A. Bostwick, T. Seyller, K. Horn, and E. Rotenberg, Controlling the electronic structure of bilayer graphene, Science **313**, 951 (2006).
[31] F. Varchon, R. Feng, J. Hass, X. Li, B. Ngoc Nguyen, C. Naud, P. Mallet, J.-Y. Veuillen, C. Berger, E. H. Conrad, and L. Magaud, Electronic structure of epitaxial graphene layers on SiC: effect of the substrate, Phys. Rev. Lett. **99**, 126805 (2007).
[32] G. Kresse and J. Furthmüller, Efficient iterative schemes for *ab initio* total-energy calculations using a plane-wave basis set, Phys. Rev. B **54**, 11169 (1996).
[33] J. P. Perdew, K. Burke, and M. Ernzerhof, Gerneralized gradient approximation made simple, Phys. Rev. Lett. **77**, 3865 (1996).
[34] P. E. Blochl, Projector augmented-wave method, Phys. Rev. B **50**, 17953 (1994).
[35] See Supplemental Material at http://link.aps.org/supplemental/10.1103/PhysRevLett.117.116102 for the detailed atomic configurations and formation energies.
[36] D. R. Lide, *Handbook of Chemistry and Physics* (CRC Press, Boca Raton, 2000), Sec. VIII.
[37] T. Middelmann, A. Walkov, G. Bartl, and R. Schödel, Thermal expansion coefficient of single-crystal silicon from 7 K to 293 K, Phys. Rev. B **92**, 174113 (2015).
[38] A. N. Mihalyuk, A. A. Alekseev, C. R. Hsing, C. M. Wei, D. V. Gruznev, L. V. Bondarenko, A. V. Matetskiy, A. Y. Tupchaya, A. Z. Zotov, and A. A. Saranin, Low-temperature one-atom-layer $\sqrt{7}\times\sqrt{7}$-In phase on Si(111) Surf. Sci. **649**, 14 (2016).
[39] A. Varykhalov, J. Sánchez-Barriga, A. M. Shikin, C. Biswas, E. Vescovo, A. Rybkin, D. Marchenko, and O. Rader, Electronic and magnetic properties of quasifreestanding graphene on Ni, Phys. Rev. Lett. **101**, 157601 (2008).
[40] M. H. Kang, S. C. Jung, and J. W. Park, Density functional study of the Au-intercalated graphene/Ni(111) surface, Phys. Rev. B **82**, 085409 (2010).